Morning-to-Afternoon Evolution of Marine Stratus Polluted by Underlying Ships: Implications for the Relative Lifetimes of Polluted and Unpolluted Clouds

MATTHEW W. CHRISTENSEN, JAMES A. COAKLEY JR., AND WILLIAM R. TAHNK

College of Oceanic and Atmospheric Sciences, Oregon State University, Corvallis, Oregon

(Manuscript received 15 September 2008, in final form 26 December 2008)

ABSTRACT

Ship tracks appearing in both the morning and afternoon Moderate Resolution Imaging Spectroradiometer (MODIS) imagery for the Pacific Ocean off the west coast of the United States were used to study the morning-to-afternoon evolution of marine stratus polluted by underlying ships and nearby uncontaminated stratus. Analyzed 925-hPa winds were used to predict the afternoon positions of ship tracks found in the morning imagery. Droplet effective radii, visible optical depths, and liquid water amounts were analyzed for morning and afternoon clouds that, based on the low-level winds, were taken to be the same clouds. As found in a previous study by Segrin et al., both morning and afternoon polluted clouds had smaller droplet radii, larger optical depths, and smaller liquid water amounts than the nearby unpolluted clouds. In contrast to the Segrin et al. study, however, the droplet effective radii decreased significantly from morning to afternoon in both the polluted and unpolluted clouds, with the rate of decrease being twice as large for the unpolluted clouds. The larger decrease in the unpolluted clouds is thought to be caused by drizzle, which is probably absent in the polluted clouds. The observations suggest that, with their slower rate of liquid loss, polluted clouds could have longer lifetimes than their unpolluted counterparts. Of interest is that clouds with similar droplet radii but smaller optical depths, and thus smaller droplet number concentrations and liquid water amounts, exhibited higher sensitivities to the effects of elevated particle concentrations and a greater likelihood of appearing in both the morning and afternoon satellite overpasses.

1. Introduction

The use of ship tracks to study how clouds respond to elevated concentrations of particles has yielded a number of insights fundamental to the aerosol indirect radiative forcing of climate. Ships under way beneath marine stratus and stratocumulus provide a source of cloud condensation nuclei (CCN). The CCN enter the clouds, increase droplet number concentrations, and reduce droplet radii. The effects manifest themselves as distinctive lines in imagery of reflected sunlight at near-infrared wavelengths (Coakley et al. 1987). Ship-track studies have demonstrated the correctness of Twomey's simple insight that haze is accompanied by increased CCN concentrations so that the water available for condensation is distributed over a larger number of droplets, making the droplets smaller but increasing the surface area that scatters sunlight and thereby increasing cloud albedos (Twomey 1974). The studies have also revealed evidence contrary to expectations that, owing to the smaller droplets, drizzle is suppressed in polluted clouds, thus allowing them to accumulate greater amounts of liquid water and achieve greater lifetimes (Albrecht 1989). Climate model simulations that include the aerosol indirect effect (Lohmann and Feichter 2005) appear to embrace the effects that enhance cloud lifetimes, but the simulations are judged to be too unrealistic to be reliable (Solomon et al. 2007). Observations of marine stratus polluted by underlying ships show, however, that polluted clouds have, on average, significantly smaller amounts of liquid water than their nearby unpolluted counterparts (Platnick et al. 2000; Coakley and Walsh 2002; Segrin et al. 2007). Ackerman et al. (2004) attributed this loss of liquid water to the higher rates of entrainment in clouds with smaller droplets. If the entrained air from above the cloud is sufficiently dry, the smaller droplets evaporate, increasing the entrainment rate and the loss of liquid water relative to the losses in the nearby unpolluted clouds.

Corresponding author address: James A. Coakley Jr., College of Oceanic and Atmospheric Sciences, 104 COAS Admin. Bldg., Oregon State University, Corvallis, OR 97331-5503.
E-mail: coakley@coas.oregonstate.edu

DOI: 10.1175/2009JAS2951.1

Segrin et al. (2007) extended the earlier studies by comparing how morning and afternoon summertime marine stratus off the west coast of the United States respond to underlying ships. In Segrin et al., the afternoon clouds were found to be ''thinner,'' having smaller optical depths and liquid water amounts than the morning clouds. The finding is consistent with the commonly held view that the sun ''burns off'' the marine layer during the day. Nonetheless, the droplet radii and the changes in droplet radii for the clouds affected by the underlying ships were found to be nearly identical for both morning and afternoon clouds. In the current study, a different approach is used to reveal differences in the responses of the morning and afternoon clouds. Here, National Centers for Environmental Prediction (NCEP) low-level winds are used to predict where ship tracks found in the morning (*Terra*) Moderate Resolution Imaging Spectroradiometer (MODIS) imagery should appear in the afternoon (*Aqua*) imagery. When successful, the relative positions of the ship tracks and the nearby unpolluted controls in the afternoon imagery are identified with the same clouds that appeared in the morning imagery some 2–3 h earlier. This approach thus allows the determination of differences in the evolution of the polluted and unpolluted clouds in response to the additional hours of sunlight. Although many of the findings reported by Segrin et al. (2007) are also found in this study, here it is found that, contrary to the earlier findings, droplet radii for both the polluted and the unpolluted clouds become smaller during the course of the day and that the rate of reduction is significantly faster for the unpolluted clouds. This finding provides new insight into the relative roles of drizzle and entrainment in reducing liquid water amounts in polluted and unpolluted marine stratus and suggests that although the polluted stratus may have less liquid water than their unpolluted counterparts, their rate of water loss is less. Consequently, the polluted marine stratus may well enjoy longer cloud lifetimes.

2. Data and analysis procedures

MODIS 1-km imagery was analyzed for the instruments on the National Aeronautics and Space Administration (NASA) *Terra* (morning) and *Aqua* (afternoon) satellites for the Northern Hemisphere summers of 2002 and 2003 and for August 2007. The observations covered daytime passes along the west coast of North America from 20° to 60°N and from 150° to 110°W. The methods used for identifying clouds polluted by underlying ships and for selecting nearby unpolluted clouds as controls were the same as those described by Segrin et al. (2007). Likewise, as in Segrin et al., a scheme that allows for partly cloudy 1-km MODIS pixels was used to retrieve the cloud properties (Coakley et al. 2005). During the summer months, the region under observation is predominately covered by low-level marine stratus with cloud-top altitudes near 1 km. NCEP 925-hPa-level winds were used to predict the locations of ship tracks found in the morning imagery for the times of the afternoon overpasses (NCEP reanalysis data were obtained online at http://www.cdc.noaa.gov). Ship tracks found to be common to both the *Terra* and *Aqua* satellite passes were identified and counted as track pairs. The track pairs were then analyzed to study differences in the evolution, morning to afternoon, of the clouds polluted by the underlying ships and the nearby clouds that were unpolluted.

Ship-track pairs were initially identified through the visual inspection of images derived from MODIS near-infrared reflected radiances. Visual inspection ensured that each ship track identified in a morning image corresponded to a track in the afternoon image and that the track was likely caused by the same ship. Owing to the different orbits and viewing geometries for the two satellites, occasionally ship tracks identified in the *Terra* observations went undetected in *Aqua*. In addition, ship tracks identified on the edges of images were often distorted and could not be visually identified as being a track from a single ship. Likewise, ship tracks identified in the morning would occasionally disappear completely or change forms altogether by the time of the afternoon pass. Despite these difficulties, several hundred ship track pairs were selected for analysis.

Once a ship-track pair was identified, the automated scheme described by Segrin et al. (2007) was used to identify 1-km MODIS pixels that contained clouds polluted by ships and then to select nearby pixels that contained uncontaminated clouds that served as controls. To produce representative sample sizes, ship tracks were divided into 30-km segment lengths in which the properties of polluted and unpolluted clouds were averaged. The length of the segments was a compromise between the need to divide the tracks into small enough sections so that the evolution of the polluted and unpolluted clouds could be studied as a function of distance from the track head (the location of the ship) and the need for a sufficient number of pixels within segments to produce representative averages for the properties of the polluted and unpolluted clouds. Also, 30 km is greater than the autocorrelation lengths of properties such as optical depth and droplet radius, which are typically 5–10 km for extensive marine stratus layers that completely cover the MODIS 1-km pixels. The averages for the 30-km segments are thus taken to be statistically independent based on tests performed by

TABLE 1. Numbers of paired ship tracks and ship-track segments that survived successive screening tests. Ship tracks were divided into 30-km segments along the portion of the track common to both satellite images as discussed in the text.

Screening	No.
Days with ship-track pairs	163
Hand-logged ship tracks in *Terra*	1510
Hand-logged ship tracks in *Aqua*	1648
Track pairs identified through visual inspection	558
Paired ship tracks used in the analysis	83
Paired segments suitable for analysis	373
Segments with polluted and unpolluted pixels having $A_C > 0.95$	195

Segrin et al. (2007). A segment was included in the analysis if it contained at least 20 1-km pixels that were identified as containing polluted clouds and at least 20 pixels on each side of the ship track that were identified as containing unpolluted clouds. Because the majority of track pairs occurred in completely overcast cloud decks, the study was limited to analyzing segments for which the cloud fraction for all of the pixels identified as containing polluted and unpolluted clouds within each segment was greater than 0.95.

Table 1 gives the total number of hand-logged ship tracks for *Terra* and *Aqua* on the days for which tracks common to both satellites were found. Also shown in the table is the number of paired ship tracks that were visually judged as track pairs, the number of paired tracks that had ship-track segments that satisfied the condition for the analysis, the total number of paired 30-km segments that satisfied the number-of-pixels criteria required for analysis, and the number of segments in which the cloud cover fraction for the pixels identified as containing polluted and unpolluted clouds was $A_C > 0.95$. The results in Table 1 show that about one-third of the hand-logged ship tracks were identified as ship-track pairs in the satellite passes. As previously noted, this reduction was primarily due to different orbits and viewing geometries for the two satellites. For example, ship-track segments with pixels that fell in regions of sun glint in either of the satellite overpasses were removed from the analysis. Cloud properties retrieved for partly cloudy pixels that fall in regions of sun glint are susceptible to large uncertainties (Coakley et al. 2005). Regions of sun glint were defined by viewing geometries for which the angle of reflection for sunlight fell within 30° of that for specular reflection from a flat surface. After ship-track pairs were visually identified and tracks with sun-glint contamination were removed, the number of paired tracks was further reduced owing to failures in the automated identification, the collocation of the 30-km segments, and the failure of the selected segments in either of the two satellite passes to meet the numbers of pixels containing polluted and unpolluted clouds that are required for analysis. Segments were visually inspected to remove those in which the pixels containing polluted clouds from one ship track fell on pixels associated with an adjacent track that were selected as being either polluted or unpolluted. Pixel identification failures typically arose when the automated scheme lacked a sufficient signal-to-noise ratio in the near-infrared reflectances to distinguish between polluted and unpolluted clouds and consequently failed to identify ship-track pixels. In the end, only about 15% of the paired ship tracks survived, providing on average about five 30-km segments per ship-track pair that satisfied the criteria for analysis. About half of these segments had pixels identified as containing polluted and unpolluted clouds with cloud cover fraction $A_C > 0.95$.

Figure 1 illustrates the sequence of steps that were used to identify clouds associated with a ship track that appeared in both the *Terra* and *Aqua* MODIS observations. The figure shows images constructed from 2.1-μm reflectances mapped to a latitude–longitude grid along with the NCEP wind field. Figures 1a and 1b (morning image in the left-hand panel and afternoon image in the right-hand panel) show several lines of relatively high 2.1-μm reflectance. The lines identify clouds that have been affected by haze from underlying ships and are referred to as ''ship tracks.'' The afternoon image shows that the ship track centered in the image clearly advanced to the west from its morning position. Likewise, the entire track drifted to the south. The displacements in the starting position and the ship track as a whole result from the propulsion of the ship and the strength and direction of the wind along the track.

Figures 1c and 1d show the hand-logged positions of the ship track and the results of the automated identification of the ship track and the nearby unpolluted controls. To examine the morning-to-afternoon evolution of cloud properties for the polluted and unpolluted clouds, NCEP 925-hPa winds were used to predict the position of the *Terra* ship track at the time of the *Aqua* pass. Because marine stratus exhibiting ship tracks typically cap boundary layers that are reasonably well mixed, winds at the 925-hPa pressure level, which coincides with a height near the middle of the boundary level, proved relatively successful in positioning morning ship tracks atop the corresponding afternoon tracks. Because the satellites passed over the region between the late morning (*Terra*) and the early afternoon (*Aqua*) local time, the wind field at 1800 UTC was used. A mean wind vector for the entire length of the ship track was obtained by averaging the NCEP wind components for the hand-logged points along the *Terra* track. The

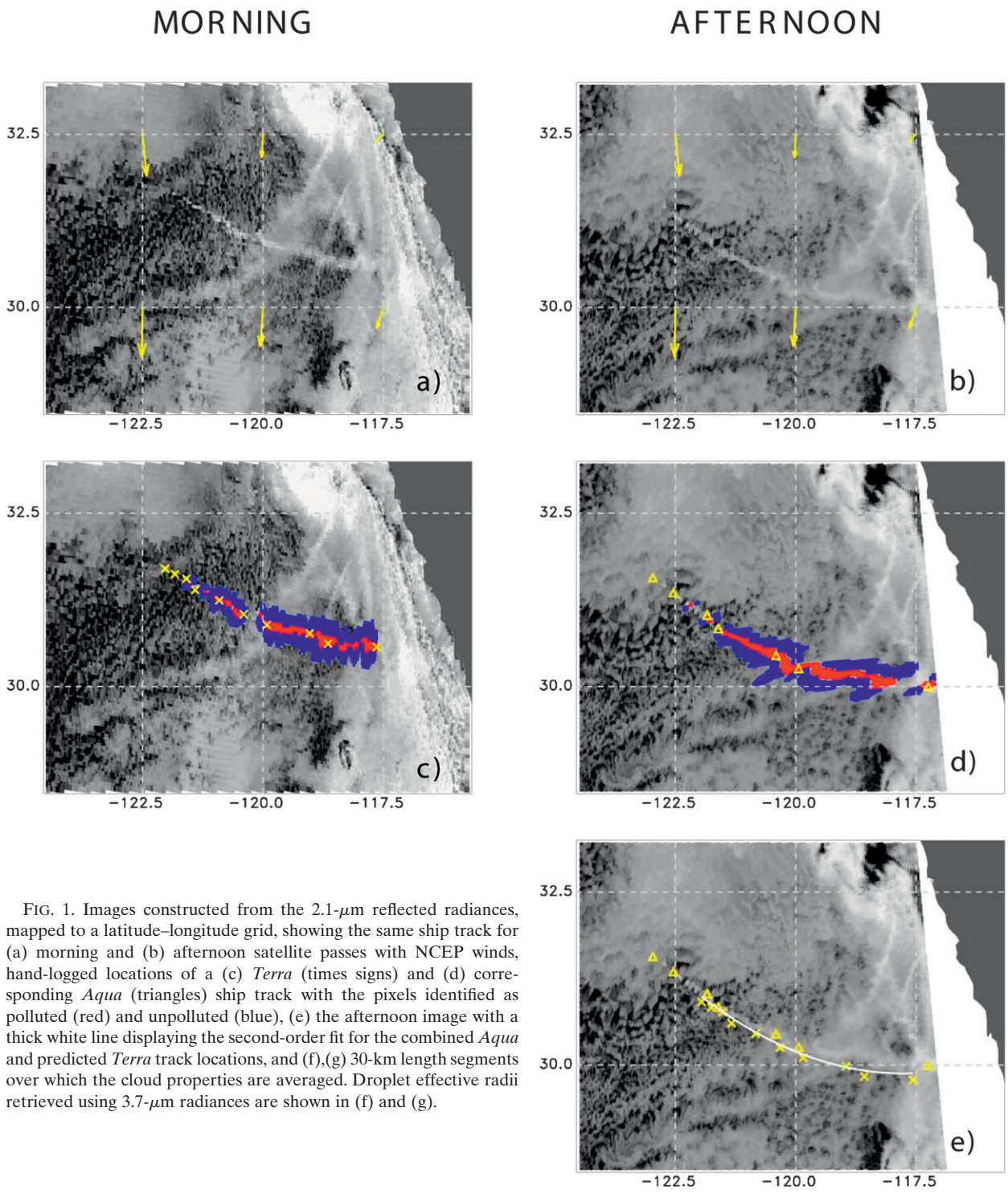

FIG. 1. Images constructed from the 2.1-μm reflected radiances, mapped to a latitude–longitude grid, showing the same ship track for (a) morning and (b) afternoon satellite passes with NCEP winds, hand-logged locations of a (c) *Terra* (times signs) and (d) corresponding *Aqua* (triangles) ship track with the pixels identified as polluted (red) and unpolluted (blue), (e) the afternoon image with a thick white line displaying the second-order fit for the combined *Aqua* and predicted *Terra* track locations, and (f),(g) 30-km length segments over which the cloud properties are averaged. Droplet effective radii retrieved using 3.7-μm radiances are shown in (f) and (g).

predicted location of the *Terra* ship track was calculated from the mean wind vector multiplied by the amount of time that elapsed between the *Terra* and *Aqua* passes.

Figure 1e shows the afternoon scene with the results of a second-order least squares fit for the combined positions of the predicted *Terra* track and the *Aqua* track. The fit is used to mitigate errors in the wind field and its interpolation. Track segments were constructed along the length of the second-order line. As the last step, the wind field was used to transfer the second-

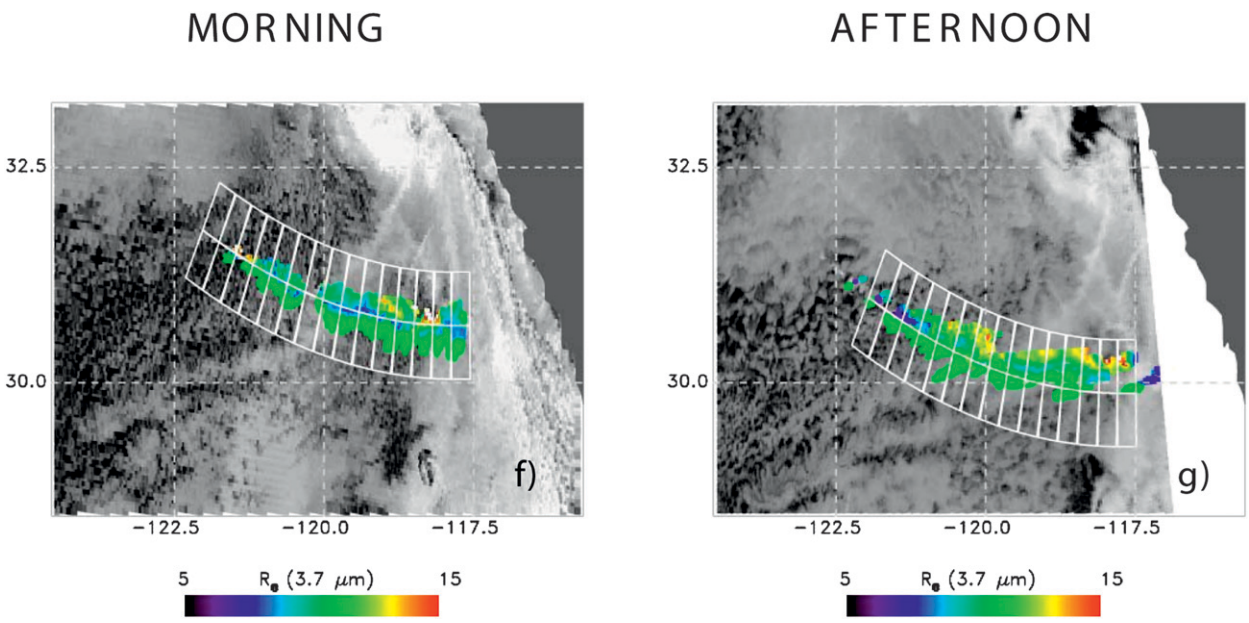

FIG. 1. (*Continued*)

order line back to the time of the *Terra* observations, thereby providing the position reference used to collocate segments common to the morning and afternoon ship tracks.

Figures 1f and 1g show the segments common to both the *Terra* and *Aqua* observations and the droplet effective radii for both the polluted and unpolluted pixels. The starting position for the construction of segments on the second-order line was based on the latitudinal and longitudinal extents of the *Aqua* and predicted *Terra* positions. Because the ship track length generally increased throughout the day, a ship track pair usually had the end of the track nearest the ship (head) of the *Aqua* track in advance of the predicted head of the corresponding *Terra* track. The starting location of the first segment was commonly located near the latitude and longitude predicted for the head of the track in the *Terra* image. The final position occurred at the end of the track farthest from the ship (tail) of either the *Aqua* or predicted *Terra* track, depending on which tail fell in a segment common to both satellites. Segment lengths along the second-order line were calculated using a great-circle distance of 30 km and the orientation of the gradient of the line within the segment. Once the segments were distributed over the length of the second-order line, ship and control pixels that fell within the bounds of the segments were analyzed. Means and standard deviations of the various cloud properties were calculated using all 1-km pixels identified as containing either polluted or unpolluted cloud that fell within the boundaries of the segments.

In this study, droplet radii and liquid water paths were derived using the 3.7-μm reflectances. Absorption by water droplets is greater at 3.7 μm than at the wavelengths of the other MODIS channels used to retrieve droplet radii (1.6 and 2.1 μm). The stronger absorption decreases the mean-free paths of photons in the clouds (Platnick 2000), thereby reducing the likelihood that the observed radiances would be as strongly affected by 3D cloud effects such as photon leakage through the sides of clouds.

3. Results

In the current study, the average solar zenith angle for *Terra* was found to be 29.6° and that for *Aqua* was only slightly smaller, 28.5°. Consequently, differences in solar heating at the times of the overpasses were small. The clouds observed by *Aqua*, however, were exposed to 2–3 additional hours of sunlight. Here differences in the evolution of the polluted and unpolluted clouds in response to the solar heating are presented.

Table 2 lists the average droplet effective radius, visible optical depth, and liquid water amount for the ensembles of morning and afternoon clouds studied by Segrin et al. (2007) as well as the averages for the clouds studied here that were found in both the morning and afternoon images. Differences between polluted and unpolluted cloud properties for both studies were statistically significant at greater than the 99% confidence level. For both studies the droplet effective radii for both the morning and afternoon polluted clouds were

TABLE 2. Means and standard deviations of effective droplet radius, optical depth, and liquid water path for both the ensemble averages (Segrin et al. 2007) and cloud-tracked averages (this study) for both the morning and afternoon clouds. The number of segments used for the ensemble averages was 659 (*Terra*) and 545 (*Aqua*), and the number of segments used for the cloud-tracked averages was 195. The morning-to-afternoon differences (*Terra* − *Aqua*) for ship and control averages as well as the polluted-to-unpolluted differences (Ship − Controls) for *Terra* and *Aqua* are the means and the standard errors of the means.

	Ensemble average (Segrin et al. 2007)			Cloud-tracked average (this study)		
	Ship	Controls	Ship − Controls	Ship	Controls	Ship − Controls
			Effective droplet radius (3.7 μm)			
Terra	10.1 ± 2.1	12.6 ± 3.1	−2.5 ± 0.1	9.9 ± 1.6	12.6 ± 2.4	−2.7 ± 0.1
Aqua	10.2 ± 2.3	12.6 ± 3.1	−2.4 ± 0.1	9.5 ± 2.1	11.8 ± 2.9	−2.3 ± 0.1
Terra − *Aqua*	−0.1 ± 0.1	0.0 ± 0.1		0.4 ± 0.1	0.8 ± 0.1	
			Optical depth			
Terra	18.6 ± 7.0	16.6 ± 7.0	2.0 ± 0.1	16.7 ± 6.2	14.6 ± 6.2	2.2 ± 0.2
Aqua	16.4 ± 6.9	14.2 ± 6.3	2.2 ± 0.1	15.1 ± 5.5	12.9 ± 5.2	2.2 ± 0.2
Terra − *Aqua*	2.2 ± 0.1	2.4 ± 0.1		1.7 ± 0.2	1.7 ± 0.2	
			3.7-μm liquid water path (g m^{-2})			
Terra	127 ± 58	139 ± 69	−12.0 ± 1.4	112 ± 52	122 ± 55	−9.4 ± 1.5
Aqua	112 ± 59	120 ± 62	−7.3 ± 1.0	99 ± 52	103 ± 50	−4.4 ± 1.3
Terra − *Aqua*	15 ± 1.4	19 ± 1.4		13.4 ± 2.0	18.3 ± 2.2	

2–3 μm smaller than those in the nearby unpolluted clouds. In addition, optical depths were larger for the polluted clouds than for the unpolluted clouds for both the morning and afternoon tracks. The means and standard deviations of the optical depths for both the polluted and unpolluted clouds in the ensembles studied by Segrin et al. (2007), however, were larger. The Segrin et al. ensembles contained many more cases because there was no requirement for the clouds to appear in both the morning and afternoon satellite passes, as was required in this study. Even though the ensemble averages had larger optical depths, the morning-to-afternoon differences in optical depth and liquid water amount were roughly the same for both studies.

Figure 2 shows the change in droplet effective radii, cloud visible optical depths, and liquid water amounts (morning minus afternoon) for the morning and afternoon polluted (SHIP) and unpolluted (CON) clouds. The figure also shows changes (morning minus afternoon) in the response of the clouds to the haze pollution (ship minus controls). Droplet effective radii decreased from morning to afternoon for both the polluted and unpolluted clouds. The average decrease in droplet effective radii for the polluted clouds was 0.38 μm whereas that for the nearby uncontaminated clouds was 2 times as large, 0.78 μm. The average reductions were greater than 3 times the standard error of the mean reductions, thereby indicating that the reductions were significant at greater than the 99% confidence level. In contrast, Segrin et al. (2007) found nearly identical average droplet radii for both the morning and afternoon ensembles of polluted and unpolluted clouds.

Figure 2 shows that for the morning ship tracks droplet radii in the unaffected clouds were considerably larger than those found in polluted clouds and that this difference was smaller in the afternoon clouds. In the morning, mechanisms for water loss in the unpolluted clouds—drizzle and entrainment of dry air from above the clouds that leads to the evaporation of droplets—exceeded the mechanisms for loss in the polluted clouds, primarily through entrainment and droplet evaporation (Ackerman et al. 2004). As the day progressed, the cloud layer thinned and, with some of the large droplets in the unpolluted morning clouds lost, presumably through drizzle, the difference in the average droplet radius between polluted and unpolluted clouds fell by the time of the afternoon overpass.

Optical depth decreased for both the polluted and unpolluted clouds as the day progressed, with slightly larger changes for the polluted clouds. The differences in the reductions, however, were not statistically significant. In line with the reductions in droplet radii and optical depths, liquid water amounts decreased for both the polluted and unpolluted clouds throughout the day but the decrease was larger for the unpolluted clouds, which lost approximately 15%. Even though polluted clouds may have smaller liquid water amounts, their slower rate of liquid water loss may ultimately lead to longer cloud lifetimes.

Interestingly, the clouds associated with ship tracks in the morning that managed to survive to the afternoon overpass had slightly smaller droplet radii (but the differences were statistically insignificant) and smaller optical depths than the ensemble of morning clouds

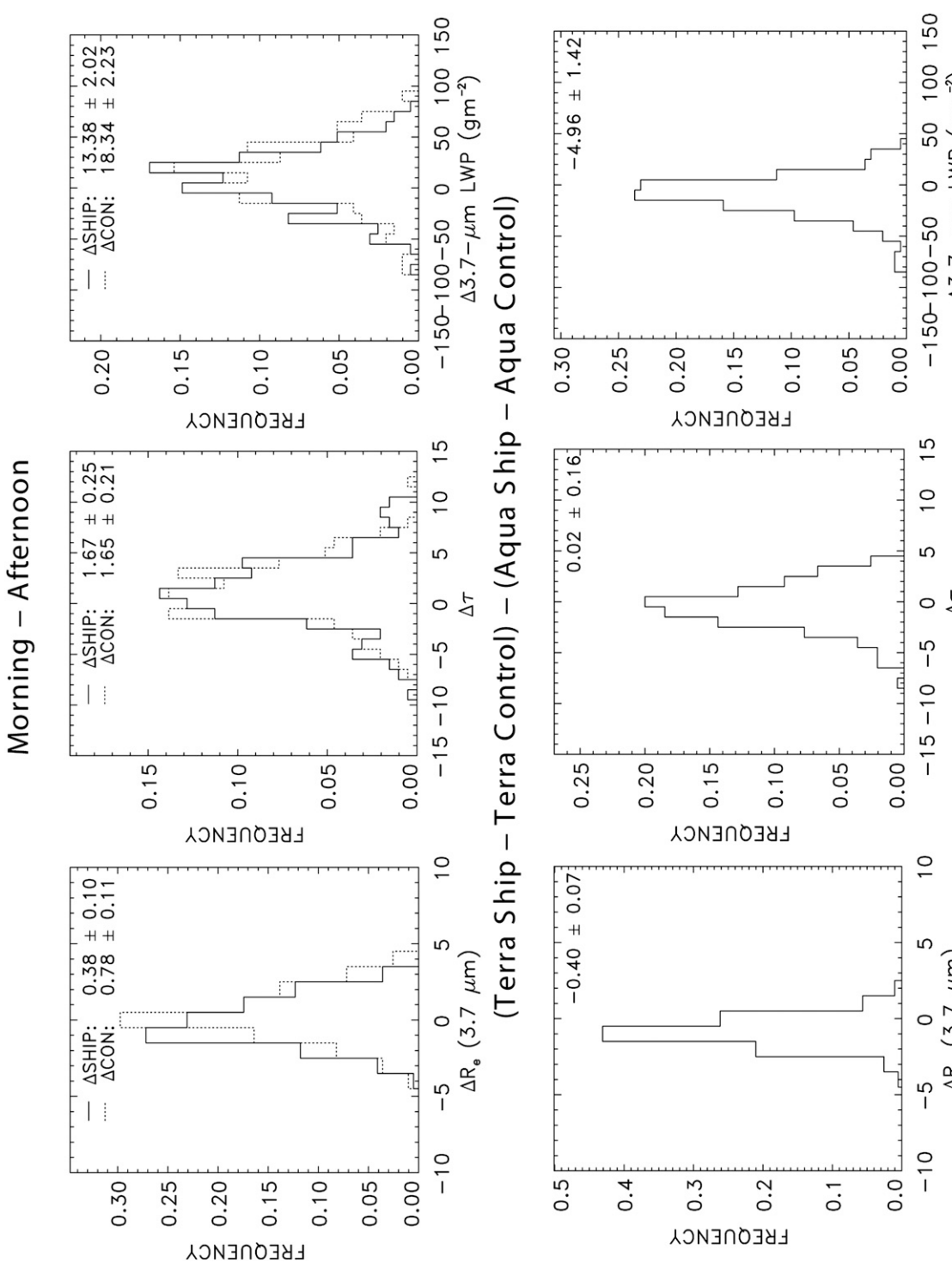

FIG. 2. Differences in droplet radii ΔR_e, visible cloud optical depths $\Delta\tau$, and liquid water paths ΔLWP (top) from morning to afternoon for the polluted clouds (ΔSHIP) and unpolluted clouds (ΔCON) and (bottom) average differences between polluted and unpolluted clouds, morning differences minus the afternoon differences. The results were obtained from the average properties in 30-km segments for the pixels identified as polluted by underlying ships and the pixels selected as nearby controls on both sides of the ship tracks. The average pixel-scale cloud fraction for pixels identified as containing polluted and unpolluted clouds was greater than 0.95 in all segments. Means and standard errors of the means are given.

studied by Segrin et al. (2007). Consequently, the clouds in the current study had smaller droplet column concentrations and liquid water amounts. In addition, they exhibited larger differences in droplet radii between polluted and unpolluted clouds than found by Segrin et al. As argued by Platnick and Twomey (1994) for clouds with fixed liquid water amounts, and as empirically demonstrated by Segrin et al. for clouds in which liquid water amounts were free to change, the morning clouds in this study were more sensitive to the effects of the particle pollution than the clouds in the morning ensemble studied by Segrin et al. Evidently, ship tracks that formed in clouds with similarly sized droplets but smaller droplet column concentrations and smaller liquid water amounts stood a better chance of being associated with a ship track in the afternoon overpass.

Because the paired ship-track segments presented different sun–target–satellite geometries for the morning and afternoon satellite passes, tests were performed to ensure that the differences between the morning and afternoon clouds were not the result of the different geometries. For example, a paired segment in the *Terra* observations was matched to another *Terra* observation that had a sun–target–satellite geometry that came closest to that obtained for the associated *Aqua* segment. The rms differences in cloud properties between the original *Terra* observations and those with the geometries closest to the corresponding *Aqua* observations were less than half of the differences found between the morning and the afternoon clouds. As a result, the effects of the different morning and afternoon geometries were deemed to be small in comparison with the differences in the morning and afternoon cloud properties reported here.

4. Conclusions

The goal of this study was to use ship tracks to compare the morning-to-afternoon evolution of clouds polluted by haze and their nearby unpolluted counterparts. Ship tracks found in the MODIS imagery for both the *Terra* and *Aqua* satellite passes over the Pacific Ocean off the west coast of the United States were analyzed for the summer months of 2002 and 2003 and for August 2007. NCEP winds were used to predict the positions of ship tracks found in the morning *Terra* imagery at the time of the afternoon *Aqua* pass. This mapping of ship tracks from the *Terra* imagery and their collocation with tracks found in the *Aqua* imagery facilitated the identification of the same clouds observed by both satellites. After identification, the properties of the morning and afternoon polluted and nearby unpolluted clouds were analyzed to determine their responses to the additional hours of sunshine. The findings for clouds tracked from morning to afternoon were compared with those obtained by Segrin et al. (2007), who studied the properties of ensembles of morning and afternoon polluted and unpolluted clouds.

In both studies, polluted clouds had larger optical depths, smaller droplet radii, and smaller liquid water amounts than the nearby unpolluted clouds. With the exception of the changes in droplet radius, both studies found decreases in optical depth and liquid water paths for both polluted and unpolluted clouds throughout the day. These reductions were the expected result of clouds thinning as a result of daytime solar heating. The largest differences between the two studies were the morning-to-afternoon changes in droplet radii. Segrin et al. found the average droplet radii to be nearly identical for the morning and afternoon clouds, whether polluted or unpolluted. Here, droplet radii in the unpolluted clouds diminished 2 times as rapidly as those in the polluted clouds during the 2–3 h between the morning *Terra* overpass and the afternoon *Aqua* overpass. The difference in the decrease was statistically significant at greater than the 99% confidence level.

In this study, the morning clouds associated with ship tracks that were also observed in the afternoon *Aqua* overpass had similar droplet radii, had smaller optical depths, and exhibited larger differences in droplet radii between polluted and nearby unpolluted clouds than found in the ensemble of morning ship tracks studied by Segrin et al. (2007). Interestingly, the clouds with the similar droplet radii but smaller droplet column number concentrations and liquid water amounts showed a greater probability of surviving the hours of sunlight from the morning to the afternoon overpass. Presumably, if the number concentration is sufficiently small, the loss of water through collision and coalescence is diminished.

The amount of water within clouds can strongly modify the aerosol indirect radiative effects by regulating cloud lifetimes. In this study, liquid water in unpolluted clouds diminished 35% more rapidly than that in the polluted clouds between morning and afternoon. Unpolluted clouds probably lost some liquid water through drizzle and some through the evaporation resulting from the entrainment of dry air from above the cloud. Because drizzle was probably suppressed in polluted clouds, liquid water was lost mainly through entrainment alone (Ackerman et al. 2004). Owing to the different rates of loss, differences in liquid water amounts between polluted and nearby unpolluted clouds were largest in the morning clouds. Because the rate of water loss is linked to cloud lifetime, the lifetimes of the polluted clouds examined in this study could be

enhanced relative to those of the nearby unpolluted clouds. Indeed, ship tracks are often found escaping from extensive decks of marine stratus and persisting through fields of stratocumulus into regions that are relatively cloud free, providing additional evidence that the polluted clouds survive as the surrounding clouds disappear.

The segment averages analyzed in this study were limited to those in which pixels identified as containing polluted and unpolluted clouds had cloud cover fractions greater than 0.95. This group represented the majority of the segments identified. Unfortunately, the number of segment pairs with cloud fractions substantially smaller than 0.95 was insufficient to further investigate lifetime effects under partly cloudy conditions.

High-spatial-resolution multispectral geostationary imagery comparable to the MODIS observations in this study would be ideal for ship-track studies of the evolution of polluted and unpolluted clouds. Hourly observations would remove some of the errors inherent in identifying the same clouds in widely separated satellite passes. In addition, the protocols for logging ship tracks require all tracks to have discernable track heads (the location of the ship; Coakley and Walsh 2002; Segrin et al. 2007). By systematically following a ship track throughout the day, ship tracks that would normally have been discarded because of the lack of a discernable head could be included based on the knowledge of the position and orientation from previous imagery. Studying ship tracks through their complete life cycle might also reveal the conditions responsible for their disappearance (presumably as a result of the clouds becoming decoupled from the boundary layer; Coakley et al. 2000). By analyzing ship tracks throughout their life cycles, the contribution of extended cloud lifetime to aerosol indirect effects might be deduced. Unfortunately, current geostationary capabilities fall short of the 1-km-resolution multispectral imagery used in this study to identify the ship tracks and characterize the properties of the polluted and nearby unpolluted clouds. Those capabilities may be available at some future date (e.g., 1–2 km in the Geostationary Operational Environmental Satellite R series), but that date appears to be years away.

Properly accounting for the effects of haze on cloud lifetimes is a difficult challenge for the climate research community. The results presented here, particularly the different rates at which droplet radii and cloud liquid water amounts fall between morning and afternoon for polluted and unpolluted marine stratus, could offer the first empirical evidence against which the performance of models used to estimate the effects of aerosols on cloud lifetimes might be assessed.

The results of the current study are restricted to ship tracks and the marine stratus in which they were found. Ship tracks offer a unique situation in which the unpolluted clouds on either side of the polluted clouds can be shown to be identical (Segrin et al. 2007). The polluted clouds are thus affected only by the elevated particle concentrations introduced by the underlying ship. Ship track studies avoid the difficulty encountered in determining the response of clouds to elevated particle concentrations on regional scales. For regional scales, the response of clouds to elevated particle concentrations must be unraveled from their response to the properties of the air masses that accompany the particles (Matheson et al. 2005, 2006). For ship tracks, the slower rate of loss in liquid water amount found for the polluted clouds in the current study suggests that the clouds may well last longer than their nearby unpolluted counterparts. Whether similar increases in longevity hold for clouds affected by regional-scale elevations in particle concentrations remains to be demonstrated.

Acknowledgments. We are grateful for the careful work performed by Matthew Segrin in hand-logging the positions of many of the ship tracks analyzed in this study. This work was supported by NASA's Radiation Sciences Program through Grants NNG04GF42G and NNX08AK07G.

REFERENCES

Ackerman, A. S., M. P. Kirkpatrick, D. E. Stevens, and O. B. Toon, 2004: The impact of humidity above stratiform clouds on indirect aerosol climate forcing. *Nature,* **432,** 1014–1017.

Albrecht, B. A., 1989: Aerosols, cloud microphysics, and fractional cloudiness. *Science,* **245,** 1227–1230.

Coakley, J. A., Jr., and C. D. Walsh, 2002: Limits to the aerosol indirect radiative effect derived from observations of ship tracks. *J. Atmos. Sci.,* **59,** 668–680.

——, R. L. Bernstein, and P. A. Durkee, 1987: Effect of ship-stack effluents on cloud reflectivity. *Science,* **237,** 1020–1022.

——, and Coauthors, 2000: The appearance and disappearance of ship tracks on large spatial scales. *J. Atmos. Sci.,* **57,** 2765–2778.

——, M. A. Friedman, and W. R. Tahnk, 2005: Retrievals of cloud properties for partly cloudy imager pixels. *J. Atmos. Oceanic Technol.,* **22,** 3–17.

Lohmann, U., and J. Feichter, 2005: Global indirect aerosol effects: A review. *Atmos. Chem. Phys.,* **5,** 715–737.

Matheson, M. A., J. A. Coakley Jr., and W. R. Tahnk, 2005: Aerosol and cloud property relationships for summertime stratiform clouds in the northeastern Atlantic from Advanced Very High Resolution Radiometer observations. *J. Geophys. Res.,* **110,** D24204, doi:10.1029/2005JD006165.

——, ——, and ——, 2006: Multiyear Advanced Very High Resolution Radiometer observations of summertime stratocumulus collocated with aerosols in the northeastern Atlantic. *J. Geophys. Res.,* **111,** D15206, doi:10.1029/2005JD006890.

Platnick, S., 2000: Vertical photon transport in cloud remote sensing problems. *J. Geophys. Res.,* **105,** 22 919–22 935.

——, and S. Twomey, 1994: Determining the susceptibility of cloud albedo to changes in droplet concentration with the Advanced Very High Resolution Radiometer. *J. Appl. Meteor.,* **33,** 334–347.

——, and Coauthors, 2000: The role of background cloud microphysics in the radiative formation of ship tracks. *J. Atmos. Sci.,* **57,** 2607–2624.

Segrin, M. S., J. A. Coakley Jr., and W. R. Tahnk, 2007: MODIS observations of ship tracks in summertime stratus off the west coast of the United States. *J. Atmos. Sci.,* **64,** 4330–4345.

Solomon, S., D. Qin, M. Manning, M. Marquis, K. Averyt, M. M. B. Tignor, H. L. Miller Jr., and Z. Chen, Eds., 2007: *Climate Change 2007: The Physical Sciences Basis*. Cambridge University Press, 996 pp.

Twomey, S., 1974: Pollution and the planetary albedo. *Atmos. Environ.,* **8,** 1251–1256.